IMPORTANCE OF MELT CLEANING PARAMETERS ON RELIABILITY OF TENSILE PROPERTIES IN A356 ALLOY

Ahmet Tigli
Metallurgical and Materials Engineering, Sinop University, 57000 Sinop, Turkey

Emin Uslu and Murat Çolak
Vocational School of Technical Science, Bayburt University, 69000 Bayburt, Turkey

Derya Dispinar
SINTEF Industry, Metal Production and Processing, 7034 Trondheim, Norway

https://doi.org/10.1007/s40962-025-01788-0

Abstract

This study examines how melt treatment and pouring temperature affect the microstructure and mechanical properties of A356 aluminum alloy. Samples were cast under degassed, non-degassed, and upgassed conditions at 725, 750, and 775 °C. Melt quality was assessed using the reduced pressure test (RPT) and the bifilm index (BI), while microstructural features were analyzed via SEM and EDS. Tensile testing and Weibull statistics were used to evaluate mechanical performance and variability. Results showed that by improper degassing the reproducibility of mechanical properties decreased regardless of hydrogen content of the melt. When bifilm index (BI) was high (> 50 mm), the ductility was lowered and caused greater variability in strength and elongation. SEM confirmed large oxide films in samples, linked to the brittle fracture. The work also highlighted the importance of melt cleaning parameters for the reliability of cast aluminum alloys regardless of the hydrogen content.

Keywords: *A356 aluminum casting, degassing, upgassing, mechanical properties*

Introduction

Aluminum and its alloys are among the most widely utilized metals in various industries due to their exceptional properties, including a high strength-to-weight ratio as well as excellent thermal and electrical conductivity. Aluminum alloys are commonly used in critical applications that require a combination of high strength and reliability, such as in the aviation and automotive industries. To achieve these performance requirements, aluminum alloys must be free from defects such as porosity and oxide inclusions. The presence of oxide layers and dissolved hydrogen in molten aluminum can lead to the formation of porosity and bifilms in the final cast product.[1–11] The presence of such defects can negatively influence the mechanical strength and overall reliability of the final cast component.[12,13] Therefore, it is essential to remove these impurities from the melt through appropriate treatment processes to ensure the integrity of the casting.

Oxide films formed on the surface of liquid metal can be drawn into the melt and folded due to turbulence during transfer from the melting furnace to the transfer ladle/holding furnace and during mold pouring. These folded oxide films, consisting of two unbonded oxide surfaces, are known as bifilms.[14] Bifilms may remain suspended within the melt.[15] These suspended bifilms may expand during solidification which was defined as unfurling by Campbell.[15]

Zhang et al.[16] investigated porosity defects in Al–Li alloys produced by sand gravity casting and vacuum casting. They found that switching to vacuum casting reduced the hydrogen concentration from 1.35 to 0.55 mL/100 g, decreased the maximum equivalent porosity diameter from

Received: 05 September 2025 / Accepted: 11 October 2025
Published online: 03 November 2025

259.46 to 68.17 µm, and lowered the overall porosity percentage from 1.139 to 0.015 %. This is most likely due to removal of oxides, simply because the air gap between the double oxide films expands under vacuum and the buoyancy increases in which the oxides are carried to the surface to be removed from the melt. Lázaro-Nebreda et al.[17,18] investigated an innovative degassing technique known as HSMC (high shear melt conditioning), which is designed to simultaneously remove dissolved hydrogen and oxide bifilms from molten aluminum. This method operates at higher rotor speeds, generating finely dispersed inert gas bubbles within the melt which actually helps to remove the oxides. As a result, HSMC enhances the inclusion removal while also minimizing both re-gassing and the quantity of inert gas required, in comparison with conventional rotary degassing methods. It was reported that the hydrogen content decreased from approximately 0.37 cm^3/100 g (without degassing) to 0.18 cm^3/100 g using tablet degassing, 0.096 cm^3/100 g with rotary degassing, and 0.07 cm^3/100 g with HSMC (high shear melt conditioning) degassing. Correspondingly, the density index was reduced from 13 % at 0.37 cm^3/100 g to 6 % at 0.18 cm^3/100 g, 2.5 % at 0.096 cm^3/100 g, and 1.5 % at 0.07 cm^3/100 g. However, the reason for the lowered porosity is possibly due to fracture of oxide film defects into more smaller pieces under the strong shear force, thus eliminating the effect of oxides forming the pores.

Gyarmati et al.[19] investigated the effects of multiple degassing using argon (Ar) and nitrogen (N_2) gases on the quality of liquid aluminum. To evaluate melt quality, they employed techniques such as reduced pressure test (RPT), computed tomography (CT), scanning electron microscopy (SEM), and K-mold analysis. Their findings indicate that argon is more effective than nitrogen in reducing porosity in RPT samples. Additionally, they noted that during the multiple degassing process, nitrogen may react with aluminum to form aluminum nitride combined with bifilms, which can negatively impact the melt quality. Gyarmati et al.[20] also investigated the effect of flux addition during rotary degassing using nitrogen gas. Their findings indicate that both techniques—with and without flux—are effective in removing hydrogen from the melt. However, in samples treated without flux, an increased formation of inclusions was observed. This phenomenon was attributed to chemical reactions occurring between the molten alloy and the nitrogen gas during the degassing process. On the other hand, Rathinasuriyan et al.[21] studied the use of argon (Ar) and nitrogen (N_2) gases in the rotary degassing process of 851 aluminum alloys. The study indicates that argon and nitrogen gases of the same purity grade exhibit nearly equal efficiency in the degassing process. The main mechanism is the physical removal of oxides when bubbles are rising in the melt. Raiszadeh et al.[22–27] had carried out extensive work on the healing behavior of double oxide films where a bubble was entrapped in the liquid and change in the bubble size was recorded and analyzed. Since the air consists of oxygen and nitrogen, the change in the bubble size was related to the consumption of oxygen and nitrogen which was reacted with aluminum melt to form oxide and/or nitride. It was reported that the incubation time for AlN formation was more than 8 hours at the melt holding in liquid state.

Olofsson et al.[28,29] reported that pores were not necessarily the winners in the fracture of aluminum castings which are considered to be visible defects easily detected by non-destructive tests such as X-ray or CT. On the other hand, the hidden (invisible) bifilms win the competition compared to pores that initiates the fracture and failure.

Objective of the Study

The purpose of this study was to evaluate the influence of degassed, non-degassed and upgassed molten A356 aluminum at three different pouring temperatures: 725, 750, and 775 °C on the microstructural characteristics and mechanical properties of separately permanent mold cast tensile bars with heat treatment. The molten aluminum conditions were considered to provide low, medium, and high hydrogen contents, respectively.

Molten quality was evaluated using reduced pressure test (RPT) samples and the bifilm index (BI) method. Weibull analysis was performed on the ultimate tensile strength and elongation values. Scanning electron microscopy (SEM) and energy-dispersive X-ray spectroscopy (EDS) were used to characterize bifilm formation and oxide inclusion on the fractured surfaces of the tensile test bars. This study helps in clarifying the relationship between BI, defect formation, and mechanical properties of separately cast tensile bars.

Table 1. Chemical Composition of the A356 Aluminum Alloy (wt%) Used in the Study

Alloy	Fe	Si	Cu	Mn	Mg	Zn	Ni	Ti	Al
A356	0.14	6.82	0.001	0.003	0.337	<0.1	0.021	0.1	rem

Testing Procedure

Commercial A356 aluminum ingots were used for preparing the melts. The chemical composition is given in Table 1.

The melting process was carried out in an electric resistance furnace using an 8-kg SiC crucible. The effects of casting temperature and hydrogen level on the tensile and microstructural properties of A356 aluminum alloy were investigated. Three casting temperatures 725, 750, and 775 °C along with three hydrogen levels (low, medium, and high) were selected as experimental parameters.

To adjust the hydrogen levels, three different treatments were applied to the molten alloy: degassing, non-degassed (no treatment), and upgassing see Figure 1 (a, b and c). The degassing process was performed by purging nitrogen gas through a graphite rotor at a flow rate of 5L/min for a duration of 10 minutes. As a result of the degassing process, the hydrogen content in the molten A356 alloy was reduced, achieving a low gas level. In the non-degassed condition, the A356 ingot was simply melted to the designated casting temperature and then held at that temperature for 10 minutes without any treatment. On the other hand, in the upgassed condition, the molten metal was heated to the desired casting temperature. Water vapor was then introduced onto the surface of the molten aluminum using an ultrasonic air humidifier while no gas was purged through the rotor. The reaction between aluminum and water vapor resulted in the formation of an aluminum oxide layer on the melt surface and the release of hydrogen gas, which subsequently diffused into the liquid metal. This process effectively increased the hydrogen content in the melt, thereby achieving a high gas level in the melt.

Samples for the RPT were poured into a preheated steel mold at 200 °C and solidified under a partial vacuum of 10mbar in a vacuum chamber. After solidification, the cross section of the RPT samples was ground and scanned for analysis. The melt quality was assessed using the bifilm index (BI), which quantifies the total length of pores as an indication of bifilm defects observed on the cross-sectional surface of the RPT samples. A lower BI value indicates higher melt cleanliness and reduced oxide film content in the alloy.

Following the collection of RPT samples, A356 aluminum alloy was cast into a tensile test mold (permanent mold, preheated to 200 °C), as schematically illustrated in Figure 2. T6 heat treatment was applied to the tensile test

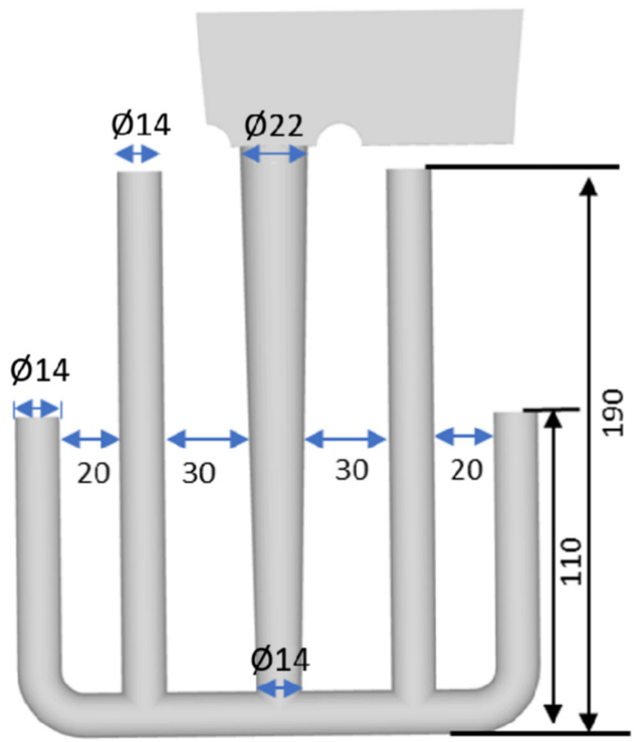

Figure 2. Dimension of the cast piece used for tensile testing.

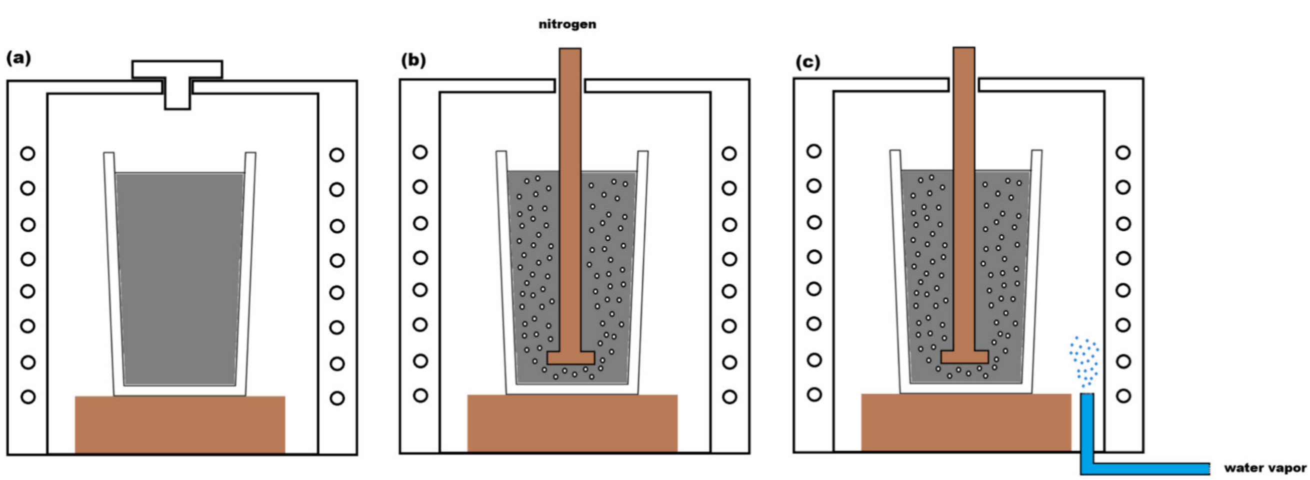

Figure 1. Casting conditions: (a) non-degassed; (b) degassed; (c) upgassed.

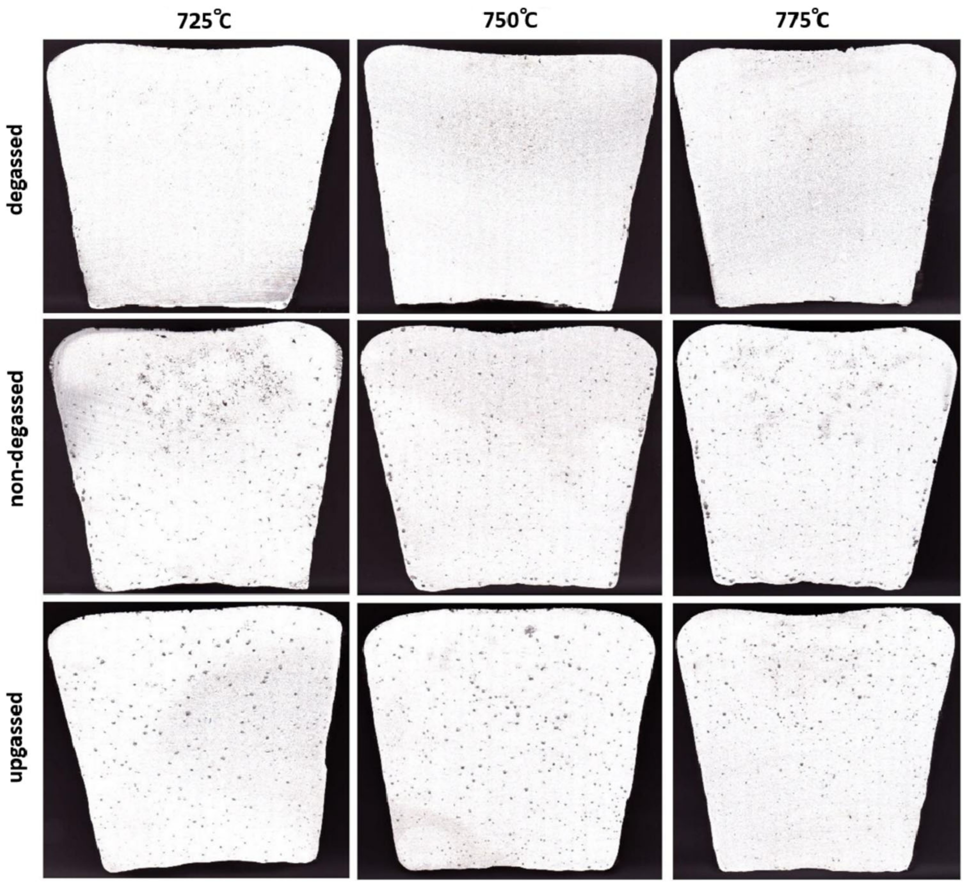

Figure 3. Cross sections of RPT samples.

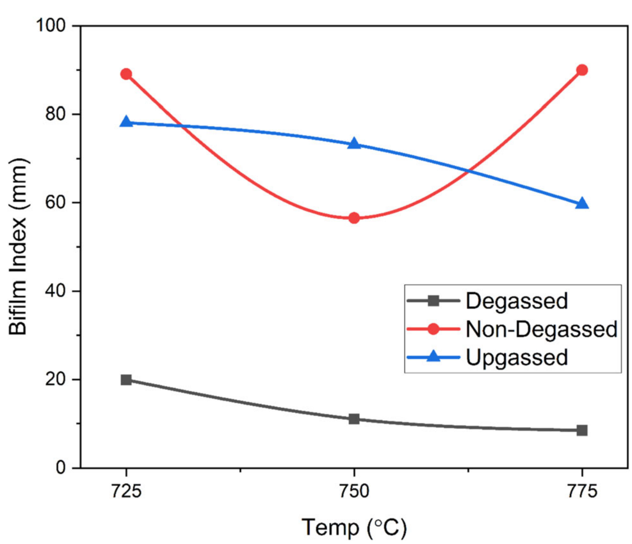

Figure 4. Bifilm index vs temp. curve of A356 alloys for all three conditions.

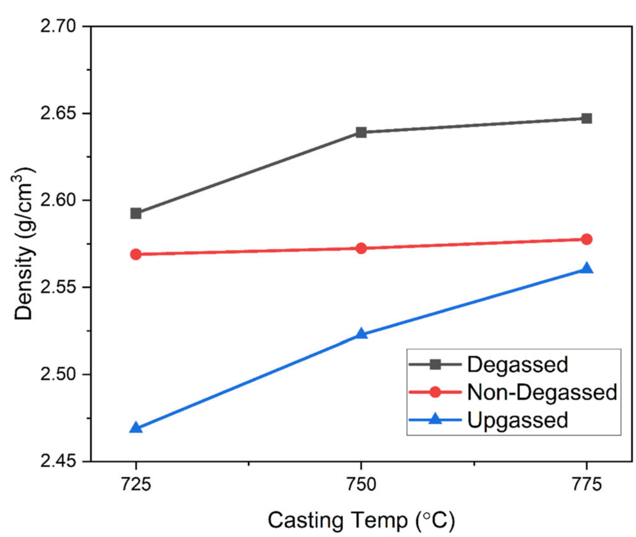

Figure 5. Density vs temperature curve of RPT samples of A356.

specimens, which included solution treatment at 540 °C for 6 hours, quenching in water at 80 °C, and aging at 150 °C for 6 hours. All bars were machined according to ASTM E8 standard. Tensile testing was conducted using an Instron 8801 universal testing machine with 1 mm/min speed. Weibull analysis was performed on the ultimate tensile strength (UTS) and elongation results.

Additionally, scanning electron microscopy (SEM) and energy-dispersive X-ray spectroscopy (EDS) were used to

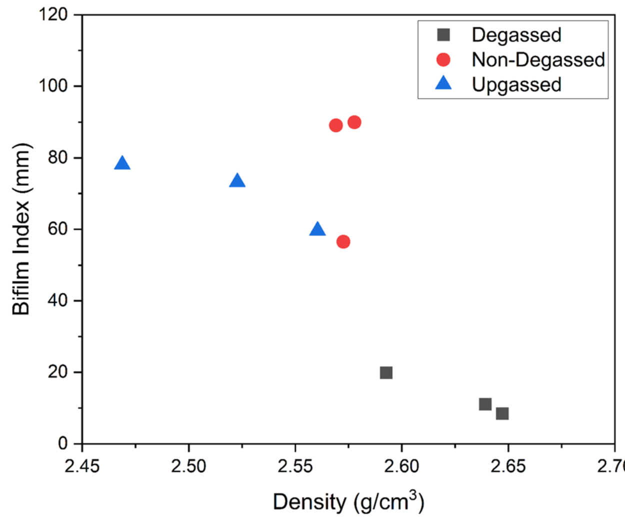

Figure 6. Density vs. BI graph of RPT samples.

characterize bifilm formation and oxide inclusion on the fractured surfaces of the tensile test bars.

Results and Discussion

This section covers the correlation between bifilm index (BI) and the density of the RPT samples. Figure 3 shows the cross sections of RPT samples, arranged in a 3×3 matrix format. The columns represent different casting temperatures (725, 750, and 775 °C), while the rows correspond to the casting conditions: degassed, non-degassed, and upgassed, respectively.

Porosities were observed on the cross section of RPT samples in all casting conditions. Degassed samples exhibit noticeably lower porosity compared to the non-degassed and upgassed samples. However, it is difficult to distinguish a significant difference in porosity levels between the upgassed and non-degassed samples based solely on visual inspection. To support these visual observations with quantitative data, BI measurements were made, as well as the densities of the RPT samples were measured using the Archimedes method.

Figure 4 illustrates the BI of RPT samples. The BI values for the upgassed and non-degassed samples range between 60 and 90 mm, whereas the degassed samples exhibit significantly lower BI values, ranging from 10 to 20 mm. These BI measurements correlate well with the visual observations of the RPT samples.

The higher BI observed in the non-degassed samples is attributed to the lower molten quality of the starting raw material and the molten bath, specifically the A356 ingots, which likely contain a higher concentration of oxide films and inclusions. In the case of the upgassed samples, the BI increases due to the introduction of water vapor, which promotes the formation of additional oxide films on the surface of the molten metal. Conversely, the degassed samples show a marked reduction in BI as the degassing process reduces both oxide film content and dissolved hydrogen in the molten metal.

As illustrated in Figure 4, pouring temperature shows an inverse correlation with the BI for both degassed and upgassed A356 samples. In degassed samples, the BI values decrease from 19.9 mm at 725 °C to 11.04 mm at 750 °C and further to 8.47 mm at 775 °C. According to the classification by Dispinar and Campbell,[30,31] molten metal can be categorized based on BI values as follows: clear melt (0–25 mm), average quality (25–50 mm), bad quality (50–100 mm), and worst quality (above 100 mm). Based on this classification, all degassed samples fall within the good melt category.

In contrast, the upgassed samples exhibit higher BI values: 78 mm at 725 °C, 73 mm at 750 °C, and 59.6 mm at 775 °C. These results indicated that the upgassed samples are associated with bad quality melts according to Dispinar's criteria. Similarly, the non-degassed samples also show BI values consistent with poor melt quality—89, 56.5, and 90 mm at 725, 750, and 775 °C, respectively. Dispinar and Campbell[32] reported that A356 castings containing 0.4, 0.2, and 0.1 ml/100g of dissolved hydrogen exhibited BI values of approximately 75, 95, and 120 mm, respectively. This was attributed to the non-optimized melt treatment during rotary degassing. Similarly, Tunca et al.[1] investigated the effects of optimized refining processes on 6060 aluminum alloys by evaluating the BI. It was shown that a decrease in BI values could be achieved with controlled degassing and cleaning in which the flow rate of nitrogen was decreased from 4 bars to 2 bars, and the degassing duration decreased from 20 to 15 minutes.

Figure 5 represents the relationship between the molten temperature and the density of the RPT samples. The degassed samples exhibit the highest densities. This trend is consistent with the observed decrease in bifilm index for degassed samples as casting temperature increases, indicating improved melt quality. It is important to note that as the melt temperature increases, oxidation increases. This may lead to the bifilms to become thicker. Therefore, the unraveling of oxides becomes harder, and they may not open-up under vacuum to reveal larger pores because of the rigidity of the thicker oxides. Thus, the bifilm index becomes lower at higher temperatures.

In contrast, the density of the non-degassed samples remains nearly constant across all casting temperatures, suggesting little variation in melt cleanliness or gas content. Upgassed samples display the lowest densities, but it increases as the molten temperature rises. These lower densities reflect the lowest melt quality due to increased

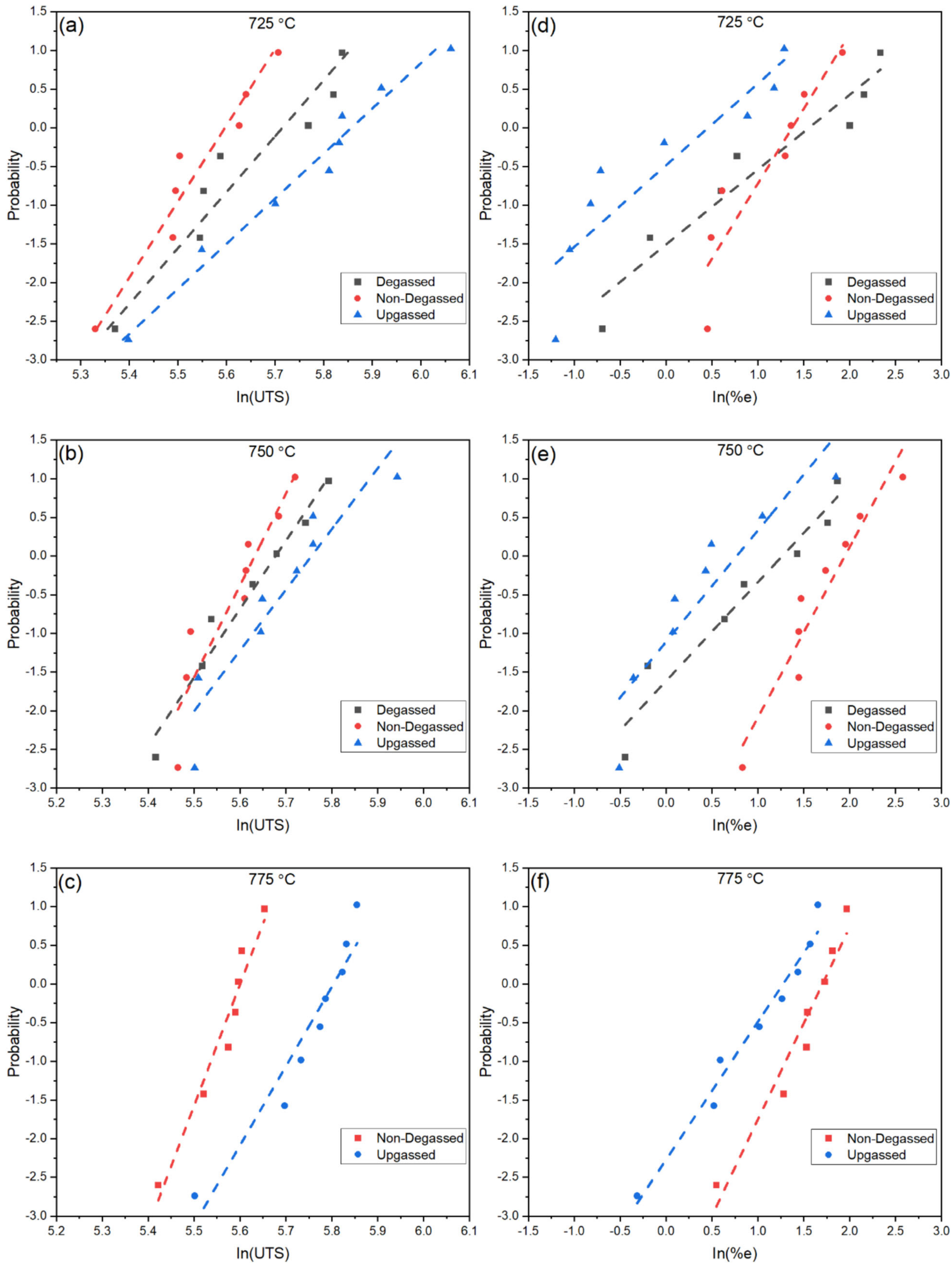

Figure 7. Weibull plot under different casting conditions.

Table 2. Weibull Analysis Results of Tensile Tests Results

Temperature (°C)	Condition	UTS (MPa)			Elongation (%)		
		Characteristic value (beta)	Weibull moduli (m)	R^2	Characteristic value (beta)	Weibull moduli (m)	R^2
725	Non-degassed	280.97	12.05	0.95	4.74	2.44	0.95
725	Degassed	322.63	8.31	0.86	7.14	1.34	0.93
725	Upgassed	382.47	9.65	0.95	2.50	1.33	0.87
750	Non-degassed	291.63	20.19	0.93	8.71	2.74	0.86
750	Degassed	305.08	11.84	0.93	4.76	2.09	0.93
750	Upgassed	337.13	9.76	0.82	3.06	1.56	0.95
775	Non-degassed	275.53	34.84	0.87	6.07	5.96	0.83
775	Upgassed	340.17	34.65	0.99	4.49	4.64	0.99

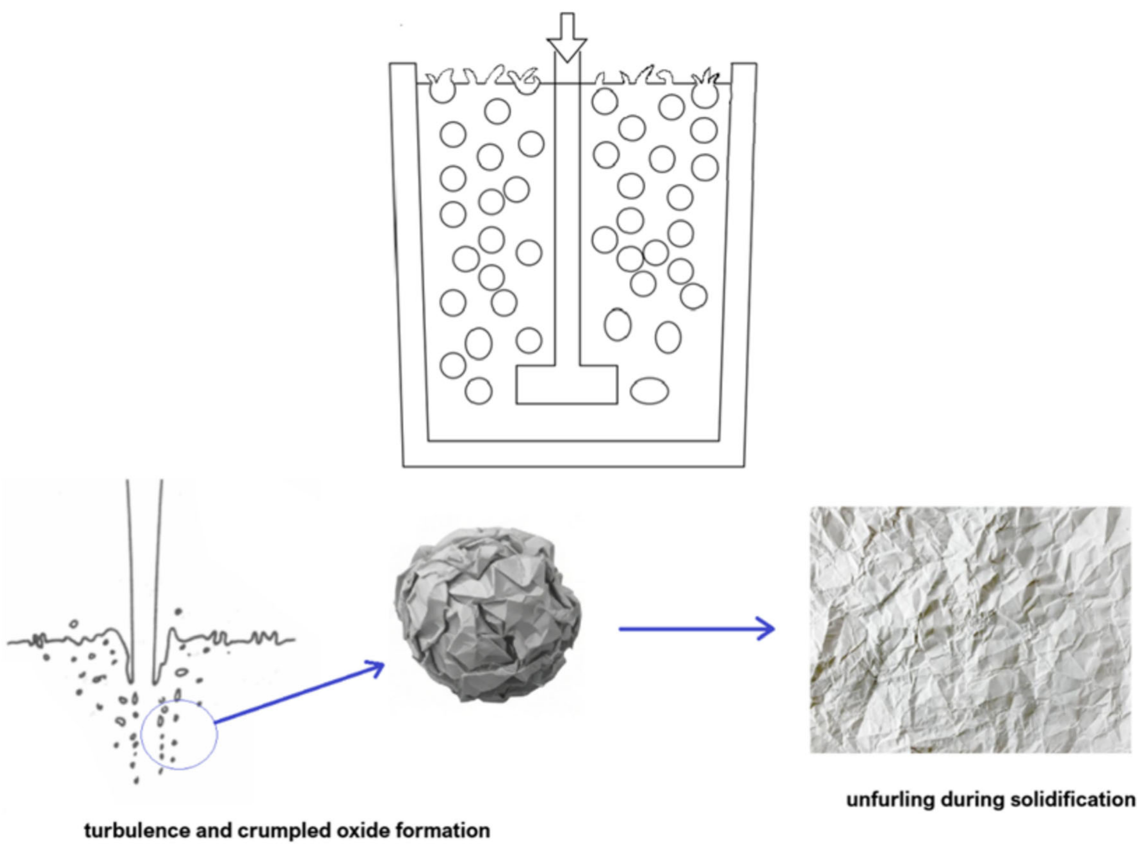

Figure 8. Schematic representation of improper degassing process.

oxide and gas content introduced during the upgassing process.

Figure 6 illustrates the relationship between BI and density for A356 RPT samples. In both degassed and upgassed samples, an inverse correlation is observed between BI and density. For the degassed samples, BI values decreased, while the corresponding densities increased. A similar trend is evident in the upgassed samples, where BI values decreased, accompanied by an increase in density.

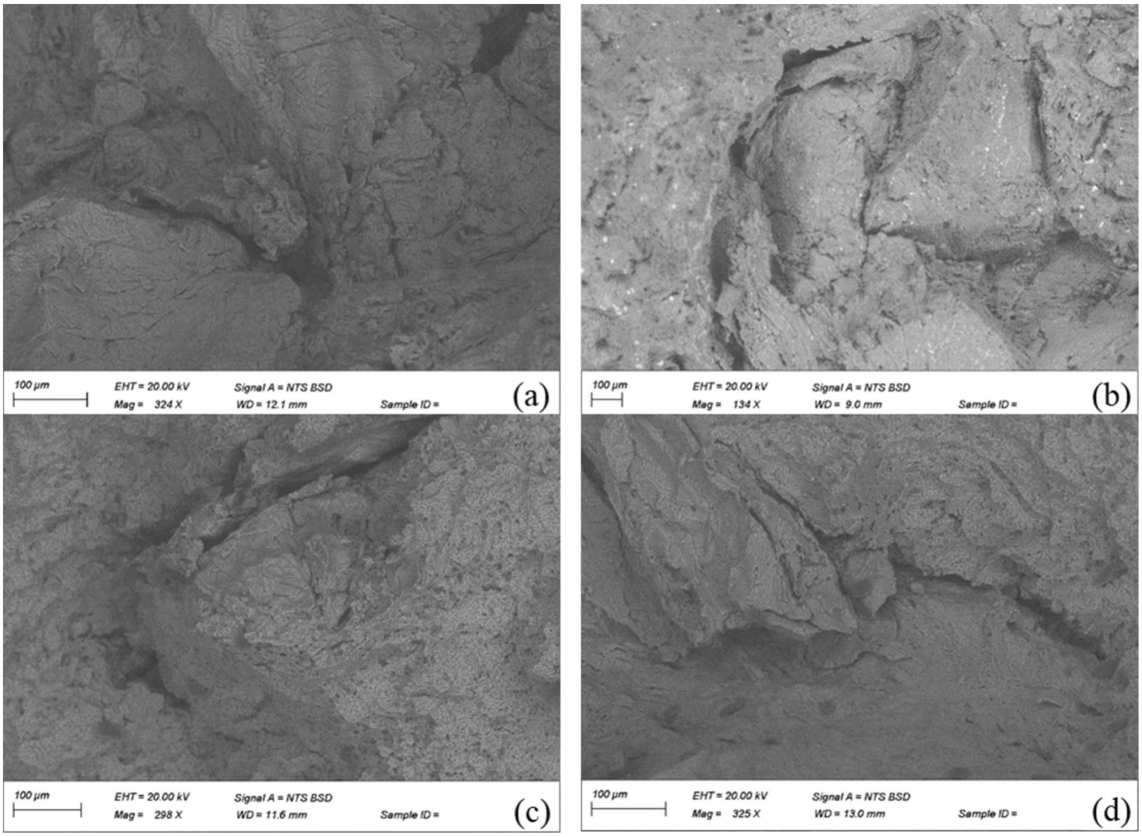

Figure 9. SEM images of the fracture surfaces of tensile bars of non-degassed castings.

In contrast, the non-degassed samples show a more scattered relationship between BI and density compared to the more consistent trends observed in the degassed and upgassed samples. This scattering may be attributed to variations in porosity morphology. Specifically, for a constant porosity volume, a decrease in pore diameter leads to an increase in BI, since smaller pores are more likely associated with entrained oxide films. The scatter of BI in the non-degassed condition clearly reveals that the quality of the melt is inconsistent. Most of these defects actually come from the raw material due to (probably) improper pouring or melt cleaning during the production of the ingots. Erzi[33] had carried out an in situ RPT test to evaluate the quality of incoming ingots. It was reported that the DC cast A356 ingots had lower porosity compared to gravity cast ingots. This was attributed to the turbulent filling of ingots during production.

Results and Discussion of Mechanical Properties

This section presents the mechanical properties (tensile test results) of A356 aluminum alloys under varying gas levels and casting temperatures. Cylindrical cast samples were subjected to T6 heat treatment. The tensile test results were analyzed using the Weibull distribution, a statistical method employed to assess the reliability and repeatability of the test samples. A linear fit has been applied to each dataset. This color scheme is consistent across all six graphs for both the UTS and elongation Weibull distribution analyses (Figure 7). All the data together with goodness to fit results are provided in Table 2.

The average UTS values for degassed samples were higher than non-degassed samples. However, the upgassed samples showed the highest average UTS values. These results indicate that casting temperature has a limited effect on the UTS properties of A356 aluminum alloy castings. This observation is further supported by the β (beta) values from the Weibull distribution analysis of UTS (Table 2).

On the other hand, the gas level has no significant influence on the Weibull modulus of UTS at a given casting temperature (Table 2). Weibull moduli were recorded to be increasing with increased temperature which was an indication that the reproducibility of the findings was increased. The Weibull modulus decreased in the order of non-degassed, degassed, and upgassed conditions, but increased with rising casting temperature. Thus, it can be clearly seen that degassing does not specifically imply that the tensile properties will be high and more reliable mechanical properties will be achieved.

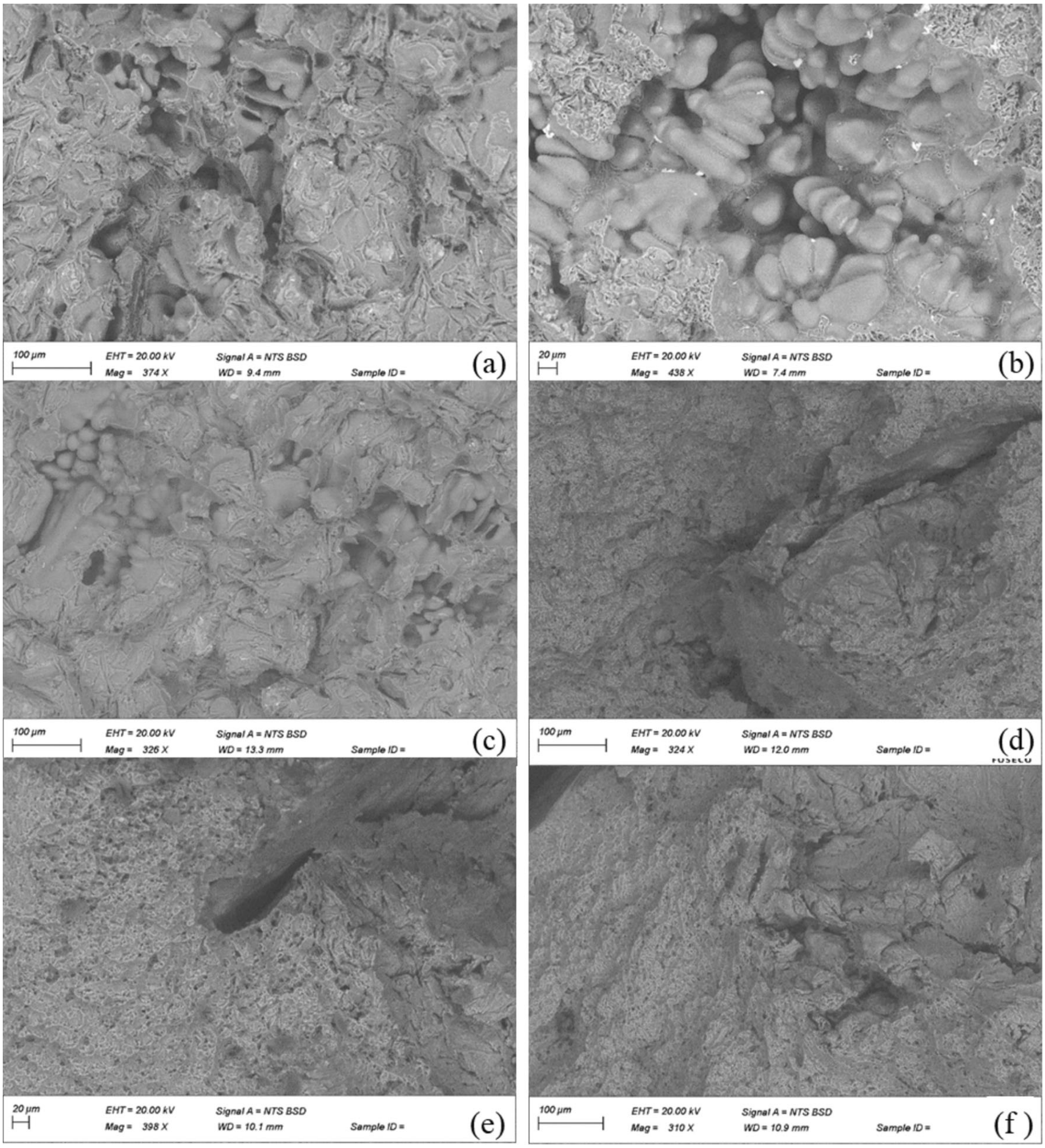

Figure 10. SEM images of the fracture surfaces of tensile bars of degassed castings.

Scanning electron microscopy (SEM) and energy-dispersive spectroscopy (EDS) analyses were conducted on A356 alloy samples subjected to various treatments (non-degassed, degassed, and upgassed) and casting temperatures. SEM images were captured from the fracture surfaces of tensile test specimens. It is important to note that all samples were heat treated together in the same furnace; therefore, the results of mechanical tests are purely representation of the effect of bifilm defects, indicating that the results were not influenced by heat treatment parameters.

Figure 8 shows the schematic representation of the aluminum degassing process where an improper degassing generates large bubbles that rise rapidly to the surface. A close-up view of how these large bubbles burst at the liquid metal's surface, introducing new oxide films into the liquid aluminum, is shown in Figure 8a. After such turbulence, the oxides become compacted resembling the crumpled paper due to motion in the liquid (Figure 8b). Therefore, their size becomes smaller. However, during solidification, either by the pushing action of dendrites and/or negative pressure generated by shrinkage, these oxides become unfurled, leading to larger defects per cross-sectional area. The analogy of a crumpled piece of paper, representing a bifilm or oxide film in the liquid metal, and the unfurled oxides were clearly observed in the fracture surface of

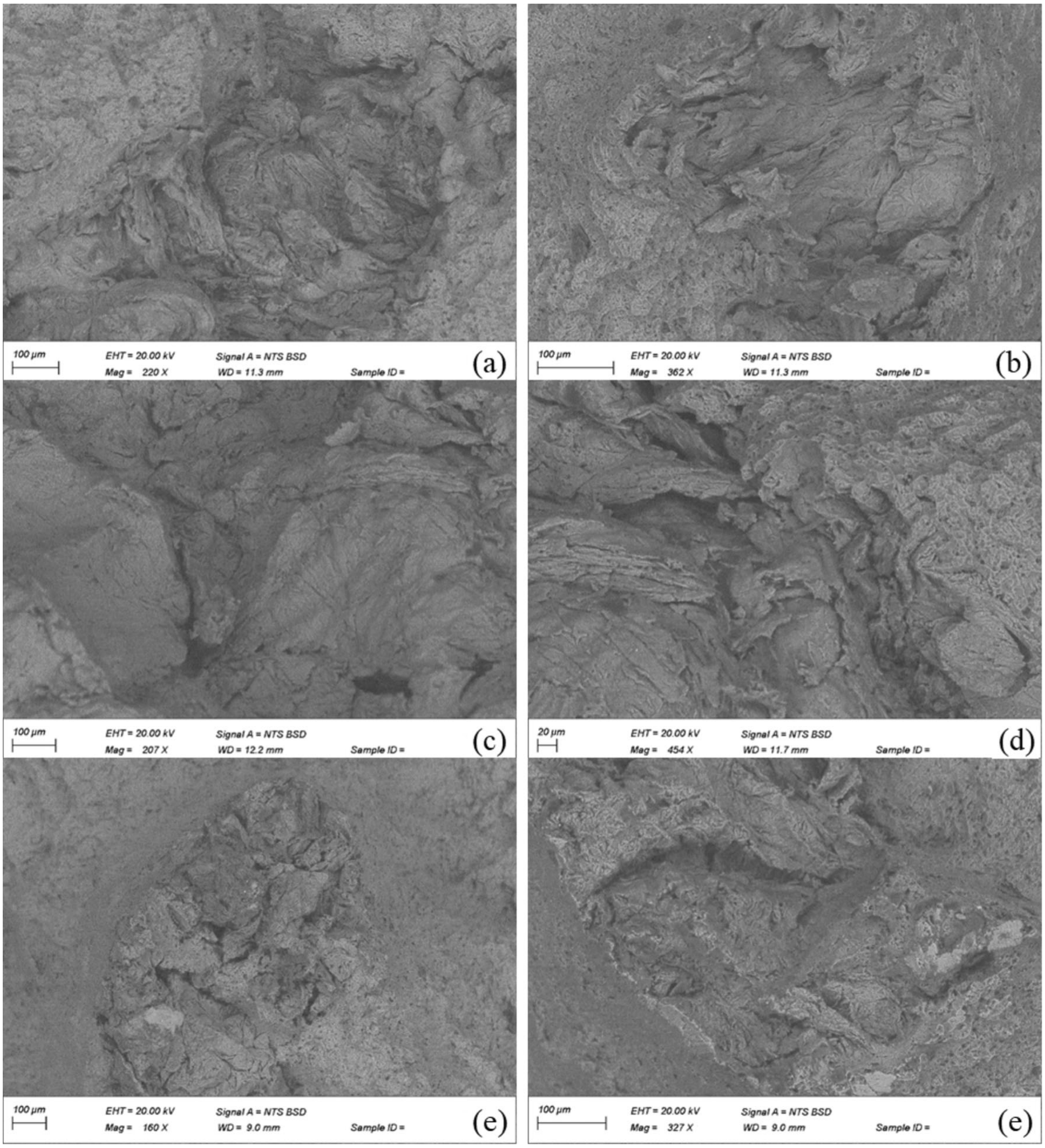

Figure 11. SEM images of the fractured surface of tensile bars of upgassed castings.

tensile bars which is summarized in Figures 9-12. Such violent degassing operation can occasionally be observed in industrial applications as in most cases it is believed that the more vigorously the melt is treated, the better the cleaning would be. However, as shown in Figure 8, this generates more oxides becoming entrained into the melt. There is also the issue of flux addition to the melt where a vortex is required to be generated in which the flux is fed into. In such applications, uncontrolled vortex generation does more harm than the aid of a flux. Therefore, to the author's experience, the proper degassing (i.e., actually: cleaning) should be carried out with the finest bubble generation during degassing with no splashing and disturbance to the melt surface. A schematic cleaning example was provided by Yorulmaz.[34] It is also important to note that there could not be a constant degassing duration for all the melts; as the quantity of oxides in the starting material might change, the duration of cleaning process needs to be adjusted based on the bifilm index measurements.

Figure 9 presents SEM images of the fracture surfaces of non-degassed tensile test bars. These images reveal a characteristic crumpled paper-like morphology associated with oxide structures, as well as microscale oxide particles. The presence of this crumpled morphology suggests the incorporation of pre-existing oxide films within the cast metal. Such oxide films exhibit a similar crumpled appearance in SEM observations (Figure 8). This indicates that the raw material (A356 ingots) may contain residual oxide bifilms formed during previous processing stages.

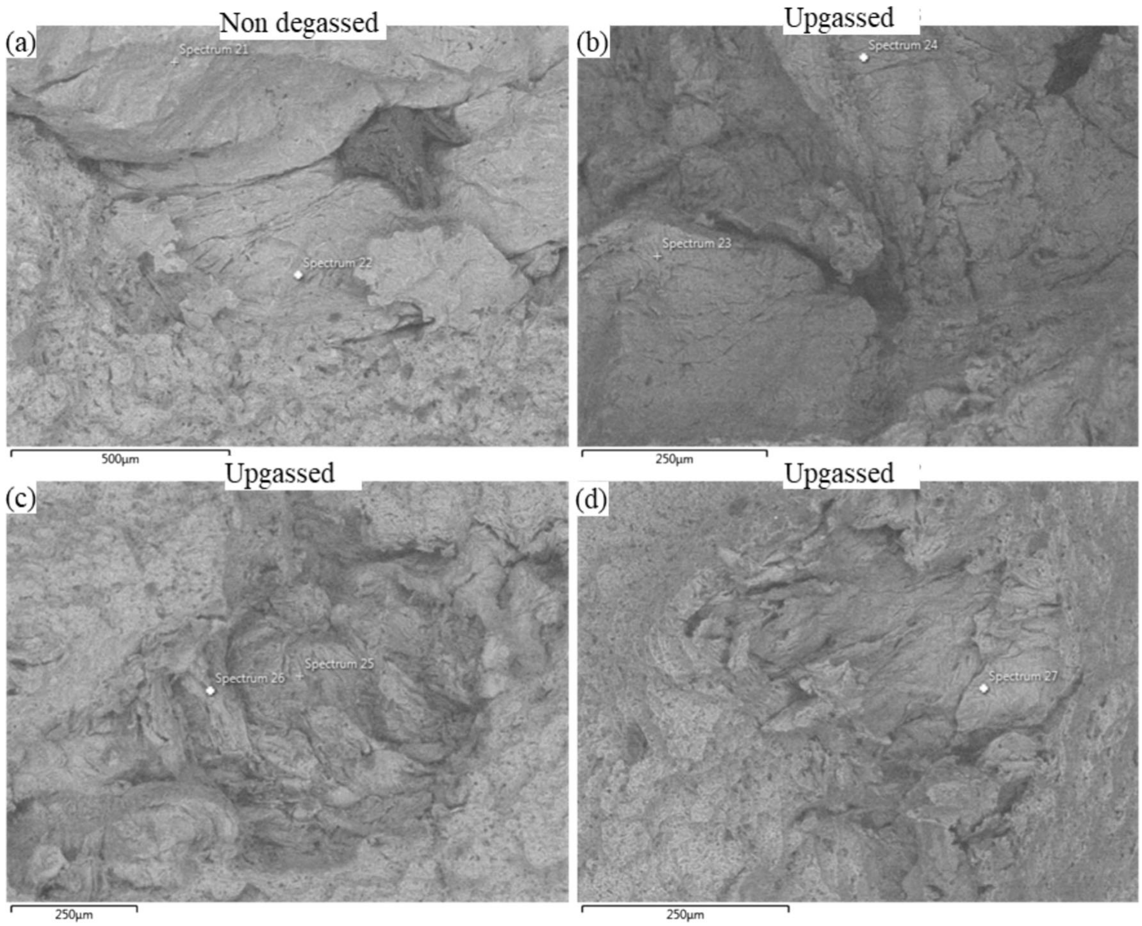

Figure 12. SEM images and EDS analyses of the fractured surface in the non-degassed and upgassed A356.

Furthermore, the non-degassed specimens exhibited fracture surfaces with crack sizes of approximately 300 µm (Figure a), up to 1000 µm (Figure b), 400 µm (Figure c), and 700 µm (Figure d). The mechanical performance of the non-degassed samples was inferior to that of the degassed counterparts. Specifically, the ultimate tensile strength (UTS) decreased from 272 MPa in degassed samples to 243 MPa in non-degassed samples produced at a casting temperature of 725 °C.

Figure 10 presents the SEM images of the degassed A356 alloy samples. In Figure 10 (a, b and c), porosities ranging from 500 to 700 µm are observed, each surrounded by a spongy-type fracture surface. Figure 10 (d and e) shows the presence of cracks—approximately 450 µm in Figure 10(d) and two cracks measuring roughly 150–180 µm in Figure 10(e)—both enclosed by spongy-type fracture morphology. In Figure 10(f), a crack of about 200 µm is visible alongside an oxide structure measuring approximately 300 µm.

Figure 11 presents SEM images of the upgassed samples. The SEM images reveal the presence of old oxide bifilms, microcracks, and microporosities. Some bifilms exhibit lengths reaching up to 600 µm, and the surface area they occupy is notably larger compared to that observed in degassed and previously non-degassed samples. Furthermore, a reduction in the spongy-type surface morphology is also observed. These microstructural characteristics may contribute to an increased brittle fracture.

Although the upgassed samples exhibit UTS values exceeding 298 MPa—higher than the average UTS of the degassed and non-degassed samples—the corresponding elongation values (1.4, 1.8, and 3.1%) are lower than those of the degassed and non-degassed counterparts. Additionally, the Weibull modulus values for the upgassed samples cast at 725, 750, and 775 °C are 0.7, 1.0, and 1.8, respectively. These values are lower than those observed in the non-degassed and degassed samples, indicating greater variability in the mechanical test results. This increased fluctuation may be attributed to the presence of large bifilms (up to 1000µm in length) and old oxide defects, as observed in the SEM images. It is also assumed that the presence of the oxides in the matrix acted like a similar behavior of a composite material, such that the UTS was increased but the ductility was suffered with low elongation. This effect is also seen in Sr-modified alloys where the oxide structure is modified from pure aluminum oxide into spinel type of $SrO.Al_2O_3$.

Figure 12 displays the SEM images and corresponding EDS analysis of the A356 samples. The figure reveals the presence of both spongy-type and crumpled paper-like structural features on the fracture surface. These morphologies are indicative of casting defects commonly associated with oxide films and inclusions. The EDS analysis (Figure 12) further confirms the presence of oxide layers and intermetallic compounds within the non-degassed samples see Table 3.

Figures 13 and 14 show the microstructure of A356 samples under different casting conditions. The first, second, and third columns correspond to non-degassed, degassed, and upgassed samples, respectively. The first row presents non-heat-treated samples, while the second, third, and

Table 3. EDS Analyses of the Fractured Surface

Alloy	Fe	Si	O	Mn	Mg	Cr	Al
Non-degassed spectrum 21	29.7	6.0	14.2	0.9	3.9	1.0	44.2
Non-degassed spectrum 22	–	6.1	12.0	–	0.5	–	81.3
Upgassed spectrum 23	–	15.5	10.1	–	1.3	–	73
Upgassed spectrum 24	–	13.6	9.7	–	1.6	–	75
Upgassed spectrum 25	–	6.6	20	–	1.8	–	71.6
Upgassed spectrum 26	–	7.7	11.8	–	1.9	–	78.6
Upgassed spectrum 27	–	10.4	29.6	–	3	–	57.1

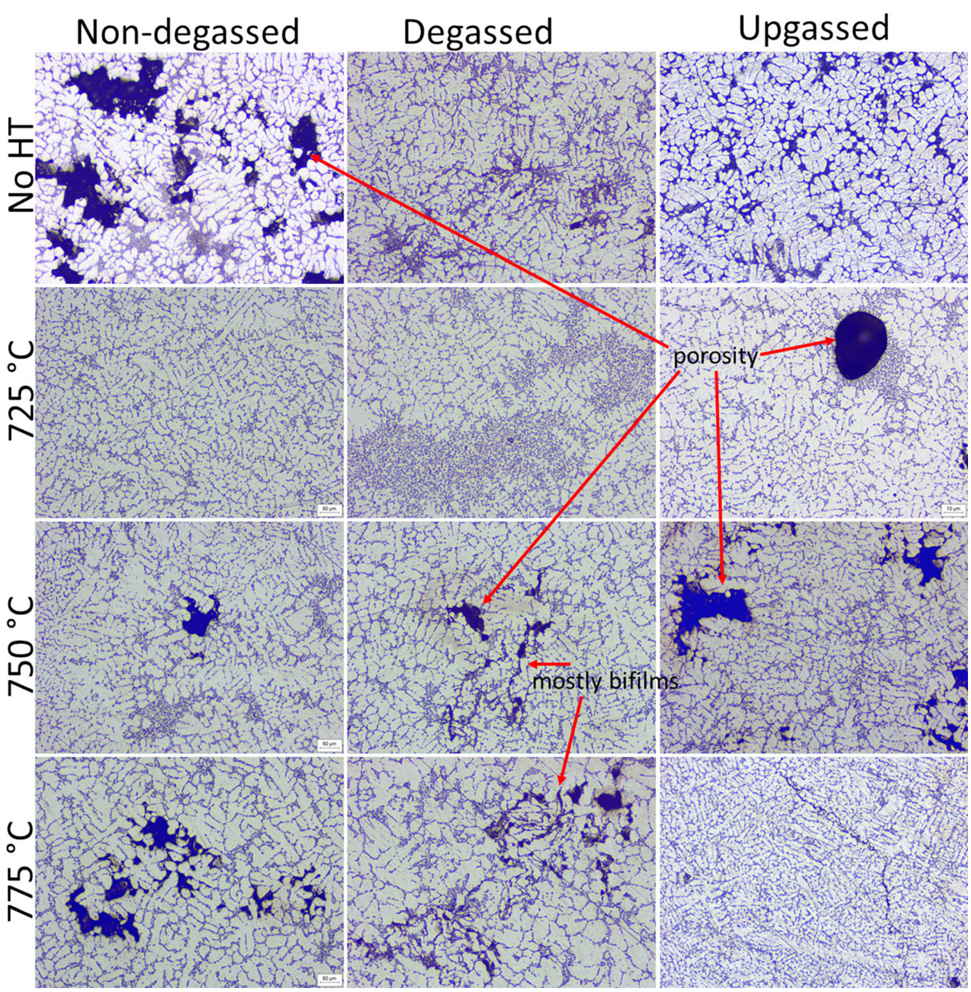

Figure 13. Optical microscope images at 100× magnification of samples.

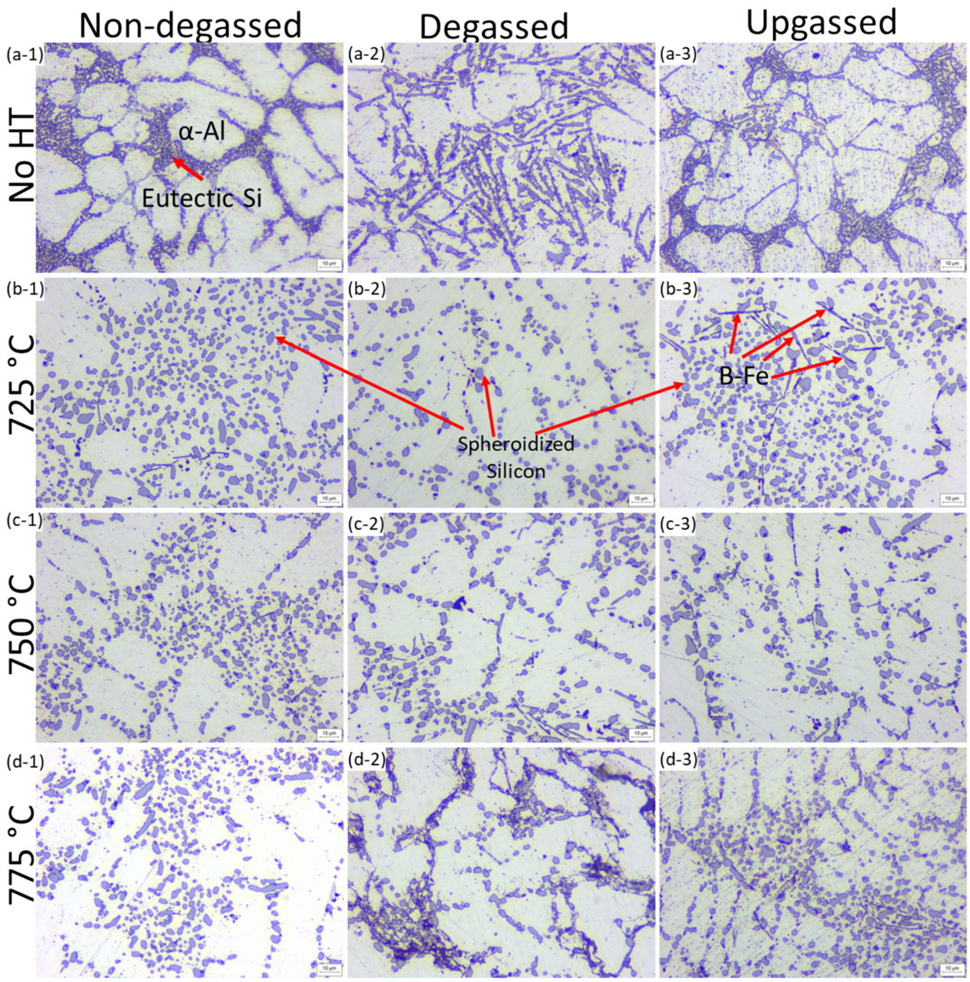

Figure 14. Optical microscope images at 500× magnification of after heat treatment.

fourth rows show heat-treated samples cast at 725, 750, and 775 °C, respectively. The microstructure of the non-heat-treated samples consists of an α-aluminum matrix, eutectic silicon, and needle-like β-iron intermetallic phases. It is important to note that the 2D of these phases is needle-like; however, they are in more complex plate-like 3D geometry. The β-Fe phase can be observed in the 500× magnification upgassed OM images. After heat treatment, the eutectic silicon phase becomes spheroidized, whereas the β-Fe intermetallic phase remains unchanged. Porosities can be clearly observed in nearly all OM images at 100× magnification. Bifilms are also visible in the degassed samples cast at 750 and 775 °C, as indicated by the red arrows.

Conclusion

In this study, A356 aluminum alloy was cast under three melt treatment conditions: degassed, non-degassed, and upgassed, at pouring temperatures of 725, 750, and 775 °C. The effectiveness of the degassing process was analyzed through the bifilm index, which was found to be affected by the degassing conditions.

It was found that the reliability of mechanical properties was affected by the shape of the entrained oxide films in the microstructure. Upgassed samples exhibited higher UTS, exceeding 300MPa, but significantly lower elongation at fracture when compared to degassed and non-degassed samples. Furthermore, the Weibull modulus values for the upgassed samples were lower in both UTS and elongation, indicating greater variability in mechanical performance. The reduced elongation suggests a more brittle fracture behavior. This is further supported by SEM observations, which reveal the presence of large, crumpled paper-like structures corresponding to old oxide films—indicative of more compact oxide bifilms that can act like a strengthening of the matrix similar to composite materials and hence very low ductility. The entrained oxides were found to originate from the surface disturbance of the melt during uncontrolled improper degassing (or upgassing) operations.

Conflict of Interest

The authors declare that they have no known competing financial interests or personal relationships that could have appeared to influence the work reported in this paper.

REFERENCES

1. B. Tunca, B. Ince, D. Deniz, Assessing melt quality in 6060 aluminum castings using bifilm and density indexes. J Mater Sci Res Rev **8**(2), 320–332 (2025)
2. Z.Z. Liu, J.H. Liu, H.M. Guo, Effects of Bi addition on bifilm of A356 casting aluminum alloy by confluence welding. Metall. Mater. Trans. B **56**(5), 5979–5995 (2025)
3. U. Kutsal, M. Colak, og O. Ertugrul, Relationship Between Aluminum Liquid Metal Quality and Defects, *Int. J. Met.*, s. 1–16, 2025.
4. M.-L. Hu og H.-M. Guo, «Entrainment Defects in Semi-solid A356 Aluminum Alloy Processed Using Slope Method», *Int. J. Met.*, s. 1–16, 2025.
5. G. Gyarmati, Á. Pálóczi, D. Somfai, T. Ferenczi, T. Mende, Z. Kéri, Analysis of different commercial solid fluxes used during the rotary degassing melt treatment of casting aluminum alloys. Metall. Mater. Trans. B **56**(1), 782–797 (2025)
6. A. Akhyar, N. Ali, M.R. Pahlevi, Variations in casting temperatures effect of re-melted 6061 aluminum alloy on tensile strength. Results Mater **26**, 100691 (2025)
7. M. Tiryakioğlu, Intrinsic and extrinsic effects of microstructure on properties in cast Al alloys. Materials (2020). https://doi.org/10.3390/ma13092019
8. M. Tiryakioğlu, The effect of hydrogen on pore formation in aluminum alloy castings: myth versus reality. Metals **10**(3), 368 (2020). https://doi.org/10.3390/met10030368
9. M. Tiryakioğlu, A simple model to estimate hydrogen solubility in liquid aluminium alloys. Int. J. Cast Met. Res. **33**(2–3), 120–122 (2020). https://doi.org/10.1080/13640461.2020.1767838
10. M. Tiryakioğlu, On the heterogeneous nucleation pressure for hydrogen pores in liquid aluminium. Int. J. Cast Met. Res. **33**(4–5), 153–156 (2020). https://doi.org/10.1080/13640461.2020.1797335
11. M. Tiryakioğlu, On estimating the hydrogen solubility in solid aluminium alloys and the hydrogen solubility difference between the liquidus and solidus temperatures. Int. J. Cast Met. Res. **34**(2), 83–87 (2021). https://doi.org/10.1080/13640461.2021.1912950
12. E. Fiorese, F. Bonollo, G. Timelli, L. Arnberg, E. Gariboldi, New classification of defects and imperfections for aluminum alloy castings. Int. J. Met. **9**(1), 55–66 (2015)
13. F. Nikolić, I. Štajduhar, M. Čanađija, Casting defects detection in aluminum alloys using deep learning: A classification approach. Int. J. Met. **17**(1), 386–398 (2023)
14. J. Campbell, The consolidation of metals: The origin of bifilms. J mater sci **51**(1), 96–106 (2016)
15. J. Campbell, An overview of the effects of bifilms on the structure and properties of cast alloys. Metall. Mater. Trans. B **37**(6), 857–863 (2006)
16. Y. Zhang, C. Xue, J. Wang, X. Yang, Q. Li, S. Wang, R. Dou, Quantifying the effects of hydrogen concentration and cooling rates on porosity formation in Al–Li alloys. J Mater Res Technol **26**, 1938–1954 (2023)
17. J. Lazaro-Nebreda, J.B. Patel, Z. Fan, Improved degassing efficiency and mechanical properties of A356 aluminium alloy castings by high shear melt conditioning (HSMC) technology. J. Mater. Process. Technol. **294**, 117146 (2021)
18. J. Lazaro-Nebreda, J.B. Patel, E. Lordan, Y. Zhang, E. Karakulak, K. Al-Helal, Z. Fan, Degassing of aluminum alloy melts by high shear melt conditioning technology: An overview. Metals **12**(10), 1772 (2022)
19. G. Gyarmati, G. Fegyverneki, M. Tokár, T. Mende, The effects of rotary degassing treatments on the melt quality of an Al–Si casting alloy. Int. J. Met. **15**(1), 141–151 (2021)
20. G. Gyarmati, F. Vincze, G. Fegyverneki, Z. Kéri, T. Mende, D. Molnár, The effect of rotary degassing treatments with different purging gases on the double oxide-and nitride film content of liquid aluminum alloys. Metall. Mater. Trans. B **53**(2), 1244–1257 (2022)
21. C. Rathinasuriyan, K. Karthik, og K. Sridhar, «Investigation of degassing on aluminum alloy by rotatory impeller degasser», *Mater. Today Proc.*, 2023.
22. S. Amirinejhad, R. Raiszadeh, H. Doostmohammadi, Calorimetric study of the oxidation of Al–Mg alloys for the prediction of healing of the double oxide film defect. J therm anal calorim **113**(2), 769–777 (2013)
23. M. Aryafar, R. Raiszadeh, A. Shalbafzadeh, Healing of double oxide film defects in A356 aluminium melt. J mater sci **45**(11), 3041–3051 (2010)
24. H. Bagherpour-Torghabeh, R. Raiszadeh, H. Doostmohammadi, Role of mechanical stirring of Al-Mg melt in the healing of bifilm defect. Metall Mat Trans B **48**(6), 3174–3184 (2017)
25. H. Mahmoodi, R. Raiszadeh, Effect of Mg on healing of bifilm defects in Zn4Al melt. Int. J. Cast Met. Res. **37**(3), 176–184 (2024)
26. F. Najafzadeh Bakhtiarani, R. Raiszadeh, Healing of double-oxide film defects in commercial purity aluminum melt. Metall. Mater. Trans. B **42**(2), 331–340 (2011)
27. A. Shafaei, R. Raiszadeh, Reduced pressure test verification of healing of double oxide film defects in Al-Mg alloys. Metall. Mater. Trans. B **45**(6), 2486–2494 (2014)

28. J. Olofsson, T. Bogdanoff, M. Tiryakioğlu, On revealing hidden entrainment damage during in situ tensile testing of cast aluminum alloy components. Mater Charact **208**, 113647 (2024)
29. J. Olofsson, T. Bogdanoff, M. Tiryakioğlu, On the competition between pores and hidden entrainment damage during in situ tensile testing of cast aluminum alloy components. Metals **14**(10), 1175 (2024)
30. D. Dispinar og J. Campbell, «Use of bifilm index as an assessment of liquid metal quality», *Int. J. Cast Met. Res.*, bd. 19, nr. 1, s. 5–17, 2006.
31. D. Dispinar, J. Campbell, Critical assessment of reduced pressure test. Part 2: Quantification. Int. J. Cast Met. Res. **17**(5), 287–294 (2004)
32. D. Dispinar, J. Campbell, Porosity, hydrogen and bifilm content in Al alloy castings. Mater. Sci. Eng. A **528**(10–11), 3860–3865 (2011). https://doi.org/10.1016/j.msea.2011.01.084
33. E. Erzi, M. Tiryakioğlu, A simple procedure to determine incoming quality of aluminum alloy ingots and its application to A356 alloy ingots. Int. J. Met. **14**(4), 999–1004 (2020)
34. A. Yorulmaz, E. Erzi, O. Gursoy, D. Dispinar, End product rejection rate and its correlation with melt treatment in direct-chill casted hot rolling slabs. Int. J. Cast Met. Res. **32**(3), 164–170 (2019)